Cost-Effective and High-Efficiency Variable-Speed Switched Reluctance Drives with Ring-Connected Winding Configuration

Xu Deng, Barrie Mecrow, *Member, IEEE*, Haimeng Wu, *Member, IEEE* , Richard Martin *and* Yaohui Gai

***Abstract*—This paper presents a novel converter topology for six-phase Switched Reluctance Motor (SRM) drives, which reduces the number of switches and diodes by half, compared with the conventional asymmetric half bridge converter, but needs no additional energy storage component. A dynamic model of a six-phase SRM is developed in the MATLAB/SIMULINK environment and conventional current chopping and angle position control techniques are applied to the proposed converter, demonstrating successful operation across the full speed range with modified conventional control techniques, lower converter losses and higher system efficiency compared with the asymmetric half bridge converter. Experimental tests comparing two versions of the proposed converter with an asymmetric half bridge are described and verify the predictions of the simulations.**

***Index Terms*—Control method, High efficiency, Low cost, Power Converter, Switched reluctance motor (SRM), Switch number.**

I. INTRODUCTION

Switched Reluctance Machines (SRMs) offer many advantages including simple and robust construction, low manufacturing cost, high reliability, high efficiency and a wide speed range, and are therefore good contenders for electric vehicle traction drives[1, 2]. In recent years they have also been developed for the aviation industry [3, 4].

However, SRMs characteristically develop pulsating torque which can give rise to significant torque ripple and acoustic noise, creating a considerable limitation [5]. Furthermore the resulting input power pulsations can necessitate a larger dc link capacitor. The torque ripple can be 70% or more in three-phase SRMs [6, 7], and 50% or more in four-phase SRMs [8, 9]. The reduction of torque ripple is an active research topic and improvement strategies include machine design optimization [10-12] and advanced control techniques [13-17]. Fundamentally, the phase number of an SRM sets the number of torque pulses per electrical cycle and so directly determines the nature of the torque waveform. Higher-phase motors have experienced some popularity in recent years due to lower torque ripple, reduced phase current for a given power rating and improved fault tolerance in comparison to conventional machines [18, 19].

Although the continued development of power electronic devices offers some support for higher phase numbers, the cost and volume of the converter, and the number of connections to the SRM, all increase with phase number. The continued use of asymmetric half bridge converter with higher phases should be reconsidered if possible. Therefore, despite the benefit to torque production, the development of SRM converters has tended towards fewer switches, fewer energy storage devices, fewer connections between the SRM and converter, and increased efficiency.

Many potential converters exist for SRMs, including the asymmetric half bridge converter[20], the H-bridge converter[21], the magnetic type converter[22] and the dissipative converter amongst others[23]. The asymmetric half bridge converter is most commonly employed, exhibiting excellent phase independence at the expense of a large number of power electronic devices, requiring two switches and two diodes per phase [20]. Of the alternatives, the H-bridge, bifilar, and dissipative converters each reduce the number of switches by half, but each has consequent drawbacks and limitations. The H-bridge converter is only suitable for four or multiples of four-phase machines [21]; the bifilar converter employs an extra inductance for each phase, which increases the converter cost and volume [22]; the dissipative converter employs extra resistance to absorb the energy stored in the phase winding, giving rise to reduced efficiency and limited scope of application [23]. Except all the conventional converters mentioned above, some application specific converter topologies for SRM are proposed [24-26], which can also be treated as the potential converters.

A method for driving a six-phase SRM from a three-phase inverter has recently been proposed[27]; an unconventional winding scheme was investigated in this context, and the resulting drive demonstrated low torque ripple and high torque density, in addition to a number of substantial benefits arising from the use of a standard converter. In particular, it was shown how additional steering diodes rectified the sinusoidal, three-phase supply to a six-phase unipolar group suitable for a six-phase SRM. However, current control is somewhat decoupled from the machine in this configuration and conventional SRM control cannot be directly implemented.

The current paper develops the advantages of the six-phase SRM, proposing a ring converter topology which facilitates the

Xu Deng, Barrie Mecrow, Haimeng Wu and Yaohui Gai are with Electrical Power Group, School of Engineering, Newcastle University, UK. (e-mail: xu.deng@ncl.ac.uk, barrie.mecrow@ncl.ac.uk, haimeng.wu@ncl.ac.uk, y.gai1@ncl.ac.uk).

Richard Martin is with Nidec SR Drives Ltd, East Part House, Otley Road, Harrogate, HG3 1PR, UK. (e-mail:richard.martin@nidec-motor.com)

application of conventional control techniques with some adjustments. By employing the same number of power devices, the novel six-phase SRM drive system can produce lower torque ripple than the three-phase SRM drive system. A dynamic control model for this proposed drive has been simulated in MATLAB/SIMULINK and the results are presented here. On this basis, a second ring converter with additional diodes is proposed for the avoidance of distortion in the current waveforms. Experimental investigation and validation of the proposed drives is presented through a range of tests on a dedicated 4.0 kW prototype SRM.

II. Candidate Converters for Six-Phase SRM Drives

Converters for six-phase SRM drives can simply be achieved by extension of conventional three-phase designs. Three candidate converters are examined, below.

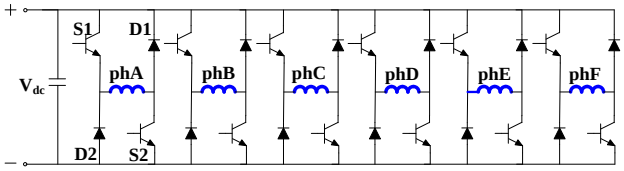

Fig. 1. Asymmetric half bridge converter for six-phase SRMs

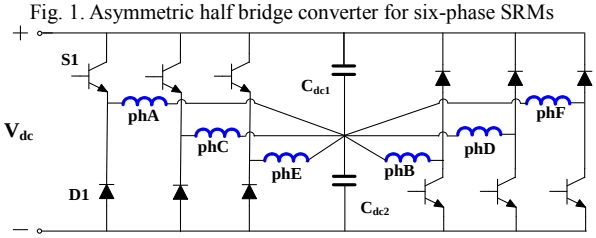

Fig. 2. Split DC link converter for six-phase SRMs

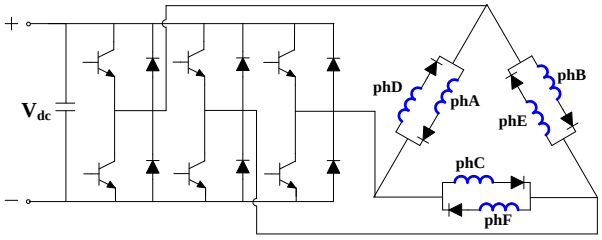

Fig. 3. Full bridge converter for six-phase SRMs

Fig. 1 shows a six-phase asymmetric half bridge converter, which is the most popular converter topology for SRM drives due to its excellent phase independence. Depending on the on-off states of two switches in each phase, there are three operating modes for each phase as summarized in Table I. This converter requires two switches, diodes, and power connections per phase; there are no additional energy storage components and the magnetization and demagnetization voltages are equal in magnitude to the DC link voltage with full phase independence.

A six-phase split DC link converter is shown in Fig. 2 referring to a two phase split DC link converter in [28]; this utilizes two equal capacitors to divide the DC link voltage in two, and one switch per phase gives rise to only two switching states per phase as shown in Table II. This converter requires one switch and diode, and potentially seven power connections between the converter and the SRM. The capacitors represent an additional energy storage requirement, and the magnetization and demagnetization voltages are half the magnitude of the DC link, which normally leads to longer commutation times.

Fig. 3 presents a six-phase SRM driven by a three-phase full bridge converter[29], in which six phase windings are arranged in a delta connection. The three-phase full bridge converter produces three-phase sinusoidal or trapezoidal currents to drive three pairs of anti-parallel phase windings. In this configuration an additional six diodes are used to convert the bipolar current waveform into two unipolar half waveforms. Note that conventional control strategies for SRMs cannot be applied with this converter topology.

TABLE I.
Operating Modes of the Six-Phase Asymmetric Half Bridge Converter

S1	S2	Phase A
on	on	$+V_{dc}$ Magnetization
on	off	Zero Voltage Freewheeling
off	on	Zero Voltage Freewheeling
off	off	$-V_{dc}$ Demagnetization

TABLE II.
Operating Modes of the Split DC Link Converter

S1	Phase A
on	$+1/2V_{dc}$ Magnetization
off	$-1/2V_{dc}$ Demagnetization

III. Proposed Converter Topology and Control Method

In order to develop the advantages of the six-phase SRM, the ideal converter has the following features:

1) Minimal number of switches;
2) Minimal number of diodes;
3) Minimal connections between the motor and converter;
4) No additional energy storage element;
5) Conventional control techniques are applicable.

None of the above candidates are fully compliant and so a new converter configuration is proposed here. Fig. 4 shows a novel converter for a six-phase SRM created from a three phase asymmetric half bridge converter.

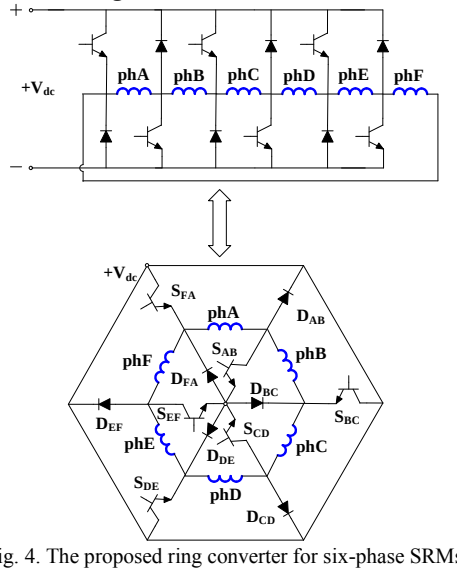

Fig. 4. The proposed ring converter for six-phase SRMs

This converter combines many of the advantages of the candidates described in section II, requiring only one diode, switch and power connection per phase, having no additional

energy storage element, and facilitating some form of conventional SRM current control. Compared to the full bridge converter of Fig. 3, the diodes placed in series with each phase are no longer required. Since the six phase windings are connected in a ring, this arrangement is subsequently named a "ring converter".

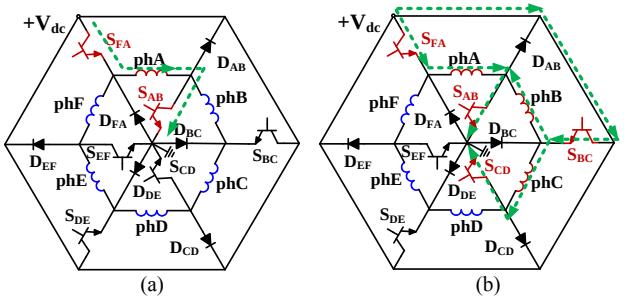

Fig. 5. Magnetization modes '+1' in the ring converter.(a) Single phase (b) three phases in parallel.

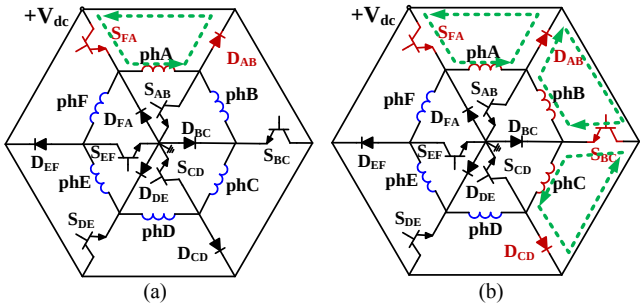

Fig. 6. Freewheeling modes '0' in the ring converter. (a) Single phase (b) three phases in parallel.

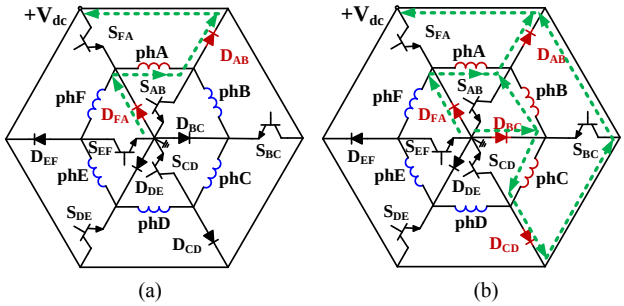

Fig. 7. Demagnetization modes '-1' in the ring converter. (a) Single phase (b) three phases in parallel.

In the ring converter, adjacent phase pairs share one switch and one power diode. For example, phase B shares its top switch S_{BC} and bottom diode D_{BC} with phase C, meanwhile, phase B shares its top diode D_{AB} and bottom switch S_{AB} with phase A. The sharing of switches between phases reduces the number of switches required but, just as in a standard three phase bridge, it also reduces phase independence, which will now be explored.

Like the asymmetric half bridge converter, the ring converter facilitates three operating modes (magnetization, demagnetization and freewheeling) in each phase, depending on the states of all six switches. These three modes are illustrated with a single phase excited in Fig. 5(a), Fig. 6(a), and Fig. 7(a) respectively. The voltage equations of these modes can be expressed:

$$\frac{d\psi_A}{dt} = V_{dc} - R_A i_A \tag{1}$$

$$\frac{d\psi_A}{dt} = -R_A i_A \tag{2}$$

$$\frac{d\psi_A}{dt} = -V_{dc} - R_A i_A \tag{3}$$

As six-phase SRMs usually have three adjacent phases conducting simultaneously, when all these phases have the same operating mode, they are connected in parallel. Fig. 5(b) illustrates the magnetization mode of three phases in parallel. Phases A, B and C are magnetized simultaneously. The positive dc-link voltage $+V_{dc}$ is applied to the parallel combination of phases A, B and C through switches S_{FA}, S_{AB}, S_{BC} and S_{CD}. The voltage equation of this operating mode can be expressed as

$$V_{dc} = \frac{d\psi_A}{dt} + R_A i_A = \frac{d\psi_B}{dt} + R_B i_B = \frac{d\psi_C}{dt} + R_C i_C \tag{4}$$

Fig. 6(b) illustrates the proposed freewheeling mode of three phases in parallel. In this mode, phase A circulates through S_{FA} and D_{AB}, phase B circulates through S_{BC} and D_{AB}, while phase C circulates through S_{BC} and D_{CD}. Therefore, there is no voltage applied on the phases. The voltage equation of this operating mode can be expressed:

$$\begin{cases} \dfrac{d\psi_A}{dt} = -R_A i_A \\ \dfrac{d\psi_B}{dt} = -R_B i_B \\ \dfrac{d\psi_C}{dt} = -R_C i_C \end{cases} \tag{5}$$

Fig. 7(b) illustrates the proposed demagnetization mode of three phases in parallel. Phases A, B and C are demagnetized simultaneously. The negative dc-link voltage $-V_{dc}$ is applied to the parallel combination of phases A, B and C through switches S_{FA}, S_{AB}, S_{BC} and S_{CD}. The voltage equation of this operating mode can be expressed:

$$-V_{dc} = \frac{d\psi_A}{dt} + R_A i_A = \frac{d\psi_B}{dt} + R_B i_B = \frac{d\psi_C}{dt} + R_C i_C \tag{6}$$

Whilst positive, zero or negative voltage can be applied to any group of phases, there are some restrictions with regard to the voltages applied to two adjacent phases. If, for example, positive voltage is applied to phase A, then Phase B must also have positive or zero volts applied: the converter topology does not permit application of positive voltage to one phase and negative voltage to the adjacent phase. The above restrictions give rise to significant phase interactions and so the application of conventional control strategies requires some adaptation.

Fig. 8 illustrates the control diagram of the six-phase ring converter using a modified current control method. In the diagram, the first two steps are similar to that of a conventional converter.

Step1: compare the phase current with the current reference value to get the current hysteresis control result.

Step 2: combine the current hysteresis control result with the firing angles to achieve the single phase switching signals.

Step 3 is further designed in order to obtain the final switching signals G_{AB} to G_{FA}. In order to guarantee enough magnetization energy, the switching signals G_{AB} to G_{FA} for the six switches in the ring converter are the logical OR operation results of every adjacent two single phase switching signals as expressed:

$$G_{AB} = G_A \| G_B \quad (7)$$

$$G_{BC} = G_B \| G_C \quad (8)$$

$$G_{CD} = G_C \| G_D \quad (9)$$

$$G_{DE} = G_D \| G_E \quad (10)$$

$$G_{EF} = G_E \| G_F \quad (11)$$

$$G_{FA} = G_F \| G_A \quad (12)$$

Where G_A to G_F are single phase switching signals for phases A to F. Hence, if there is a positive demand for either phase A or phase B, then G_{AB} is high and switch S_{AB} is on.

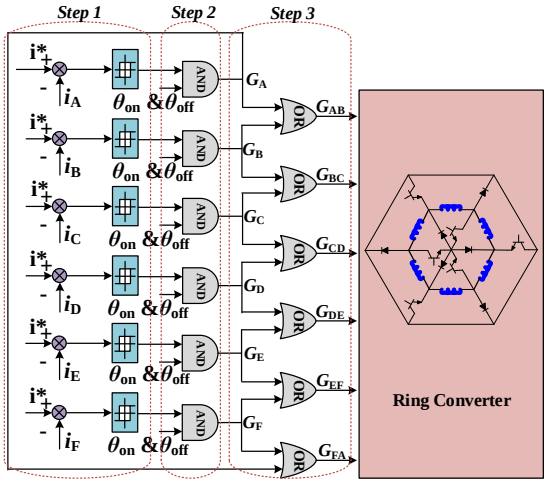

Fig. 8. Control diagram of six-phase ring converter under modified current control method

IV. Simulations

A dynamic model of a six-phase SRM was developed in the MATLAB/SIMULINK environment for simulation of the proposed ring converter and a six-phase asymmetric half bridge converter. The model used experimentally measured electromagnetic parameters from a prototype six-phase, 12/10 SRM, and the parameters are shown in Fig. 9.

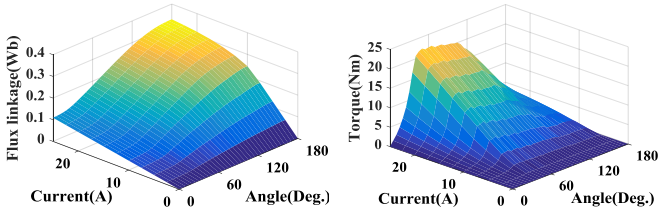

(a) (b)

Fig. 9. Measured nonlinear electromagnetic characteristics of a six-phase SRM prototype. (a) Relationship between rotor position, current and flux-linkage. (b) Relationship between rotor position, current and torque.

A. Current Control

In order to compare the performance of the converters at low speed, current chopping control strategy is applied at 200rpm. The phase reference current is 15 A, the turn-on and turn-off angles are 0° (unaligned position) and 160° respectively, and the DC link voltage is 200 V.

Fig. 10 shows the six phase current waveforms under current control, comparing the asymmetric half bridge converter with the ring converter. The phase currents of the asymmetric half bridge converter are approximate square waveforms and have 60° offset between two adjacent phases, Fig. 10(a). The current waveforms of the ring converter, Fig. 10(b), exhibit some distortion by comparison, namely an increasing current midway through the conduction period and a pronounced tail current after turn-off. Although the current distortion increases the maximum current rating of the DC link, it does not make torque output inferior, conversely, the ring converter produces higher average torque and lower torque ripple as shown in Fig. 11. The torque output difference between these two converters is generated by the increasing current midway which helps the ring converter avoid the low output in each conduction period (encircled in purple in Fig. 11).

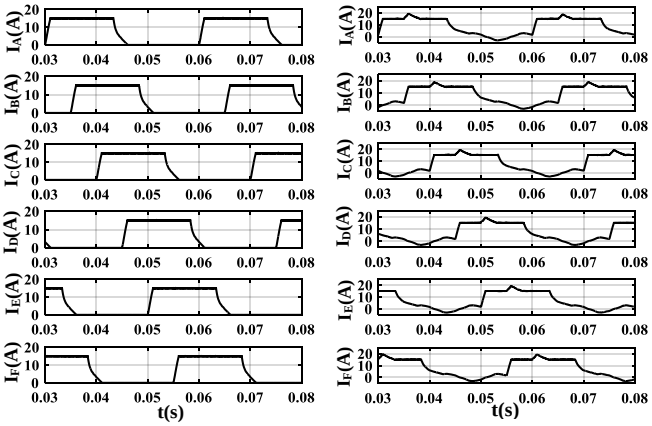

(a) (b)

Fig. 10. Simulation results of six phase currents under current control. (a) Asymmetric half bridge converter. (b) Ring converter

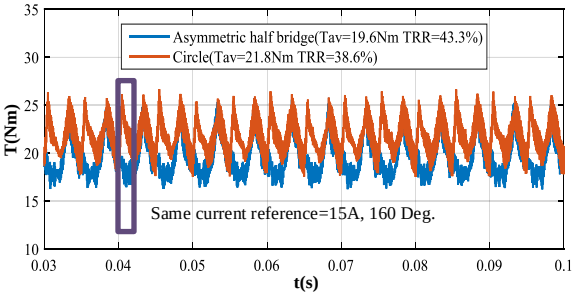

Fig. 11. Torque comparison between AHB converter and ring converter under current control

These distortions arise from the phase interdependence which is characteristic of the ring converter. For example, consider the time when phase B has been conducting for 60° and is midway through its conduction period. Phase C commences its excitation period with the closure of switch S_{BC}. Positive voltage is applied to Phase C and the state of phases B and A are dependent upon switch S_{AB}. If positive voltage is applied to phase A through closure of S_{FA} and S_{AB} then positive voltage is also applied to phase B, irrespective of whether it is required. This situation continues until Phase C reaches its demanded current, and so the current in phase B continues to increase, unless phase A is switched off. In summary, the voltage applied to the incoming and outgoing phases affects the conduction state of the intermediate phase, owing to the conduction overlap between the three phases.

The angle position difference between incoming phase N and outgoing phase (N+2) is calculated by (13). As analyzed above,

as long as phase N and phase (N+2) do not overlap, equation (14) is fulfilled and the distortion current around 60° can be avoided.

$$\Delta\theta_{\mathrm{N(N+2)}} = \theta_{N+2} - \theta_N = \frac{360°}{6} \times (\mathrm{N}+2-\mathrm{N}) = 120° \tag{13}$$

$$\theta_{con} < \Delta\theta_{\mathrm{N(N+2)}} = 120° \tag{14}$$

In order to verify how the conduction width affects the current distortions around 60°, the following simulations are conducted. Varying the conduction width of the ring converter from 80 ° to 160 °, different current waveforms can be subsequently observed and compared. Fig. 12 compares phase current waveforms under different conduction widths in verification of this analysis. Varying the conduction width of the ring converter from 80° to 160°, it can be seen that current distortion is not present where the conduction width is less than 120°as suggested by the analysis.

Limiting the conduction to 120 ° can prevent current distortion around 60°, however a pronounced tail current after turn off can still be observed in Fig. 12 and may cause extra loss for the whole system. The reason for the current distortion after turn-off is once more the special winding connection topology of the ring converter. In order to explain this, a control instant of the ring converter is picked out and shown in Fig. 13.

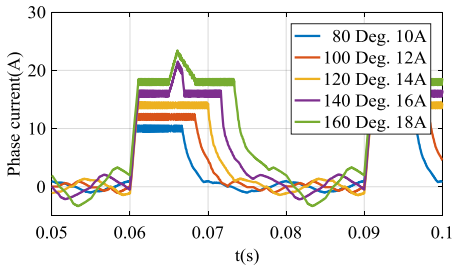

Fig. 12. Phase current with different conduction widths in the ring converter

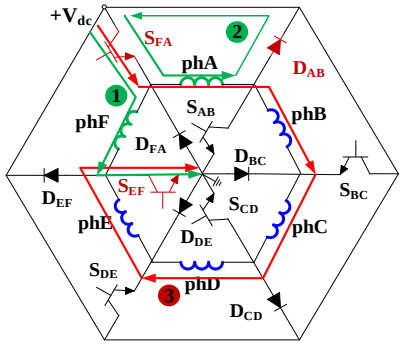

Fig. 13. Current loops in the Ring converter for six-phase SRMs

At this instant, only phases A and F are conducting, assuming application of the 120° conduction limit. When phase F is in the magnetization state (green loop 1) and phase A is in the freewheeling state (green loop 2), switches S_{EF} and S_{FA} are "on" and all other switches are "off". Five phases A, B, C, D and E are now connected in series with the DC link (red loop 3).

Phase E has just finished its conduction phase and is now switching off. However, because phase F has positive voltage applied via switch S_{EF} then phase E cannot have negative voltage applied at the same time, so its rate of current decay is reduced, resulting in the tail current.

Since phase A is freewheeling, ignoring back-EMF under current control, application of Kirchhoff's voltage law gives:

$$\begin{aligned} V_{dc} &= -u_B + u_C - u_D + u_E \\ &= -L_B(\theta)\frac{di_B}{dt} + L_C(\theta)\frac{di_C}{dt} - L_D(\theta)\frac{di_D}{dt} + L_E(\theta)\frac{di_E}{dt} \end{aligned} \tag{15}$$

The distortion current can be expressed:

$$-i_B = i_C = -i_D = i_E = i_{dist} \tag{16}$$

Substituting (16) into (15) gives:

$$i_{\mathrm{dist}} = \frac{\psi_o + \int V_{dc}\,dt}{L_B(\theta) + L_C(\theta) + L_D(\theta) + L_E(\theta)} \tag{17}$$

where Ψ_o is the original flux linkage existing in phases B, C, D and E. Assuming Ψ_o=0, the distortion current is proportional to the volt-seconds applied, and it is in inverse proportion to the total inductance of these four phases.

Table III gives the switching and phase conduction states for phases A and F over a single electrical cycle, indicating the presence of current distortion.

TABLE III.
RELATIONSHIPS BETWEEN SWITCHES AND PHASE STATE IN ONE ELECTRICAL PERIOD

S_{EF}	S_{FA}	S_{AB}	*Phase F mode*	*Phase A mode*	*Current Distortion*
off	off	off	-1	-1	no
off	off	on	-1	0	yes
off	on	off	0	0	no
off	on	on	0	+1	yes
on	off	off	0	-1	yes
on	off	on	0	0	no
on	on	off	+1	0	yes
on	on	on	+1	+1	no

Since two phases are conducting, three switches are active and therefore there are eight switch conduction combinations. It is clear that there is no current distortion when then conduction states of the two phases under consideration are the same, since there is no voltage drop across the four other phases. However, the conduction states of adjacent phases cannot always be equal and so the conditions for current distortion are unavoidable.

A simple way to solve the problem shown in Fig. 13 is to connect a power diode in series with each phase winding to restrict the directions of the phase currents. This solution is shown in Fig. 14.

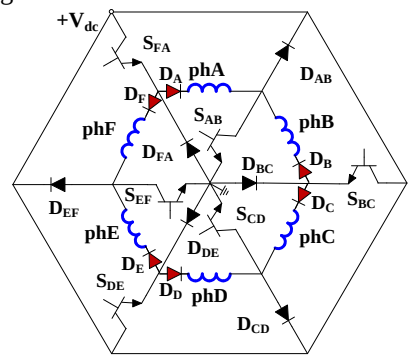

Fig. 14. Ring converter with additional diodes for six-phase SRMs

Fig. 15 shows the current waveforms in the ring converter

with additional diodes. Current distortion is no longer present owing to the conduction width limitation and the presence of additional diodes. However, the extra diodes increase the conduction losses and the component count.

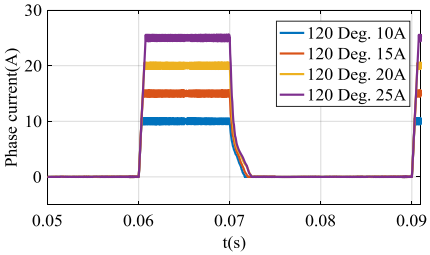

Fig. 15. Current waveform of the ring converter with additional diodes

B. *Voltage control*

In order to compare the performance of the proposed converters under voltage control, an angle position control strategy is applied at 1500 rpm. The DC link voltage is 200 V, the conduction width is 80°, and the advance angle is 0°. Fig. 16 compares the phase voltage and current waveforms from the ring converters with those from the asymmetric half bridge converter under voltage control.

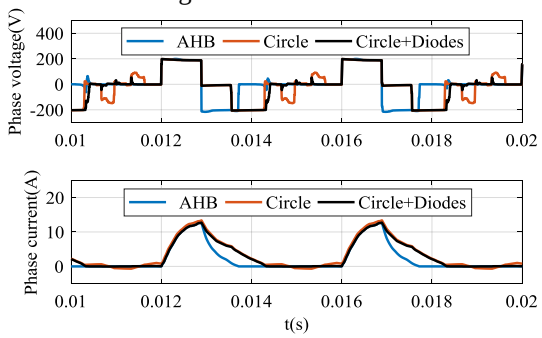

Fig. 16. Phase voltage and current waveform under voltage control.

Some differences in the voltage waveforms may be observed, since each phase of the ring converters has 80° of positive applied voltage for magnetization, followed by 60° freewheeling at zero voltage (owing to overlap between adjacent phases), followed by 80° of negative voltage for demagnetization. However, the simulation of the ring converters give reasonable current waveforms indicative of satisfactory application of voltage control.

C. *Performance comparison*

Precise control requirements generally mean that SRM drives tend towards high switching frequencies, which increases the impact of switching losses under current chopping control. In order to compare the output performance of the proposed converter (with and without the additional diodes) with the asymmetric half bridge converter, the following simulation parameters are chosen: the reference torque output T_{av} of the SRM is 20 N·m at 200 r/min, 15 N·m at 800 r/min and 10 N·m at 1500 r/min. IGBT models are employed for three converters. The control frequency is 20 kHz, the conduction width is 160° with the asymmetric half bridge converter and the ring converters. Comparison results including switching losses are shown in Table IV.

The ring converter without extra diodes has the smallest overall device losses owing to the reduced switch and diode count; this is particularly in evidence in current chopping mode at the lower end of the speed range owing to the reduced switching losses. However, when the extra diodes are included, the ring converter exhibits increased loss overall owing to the additional continuous diode conduction loss, P_d.

TABLE IV.
SIMULATED CONVERTER PERFORMANCE COMPARISON

	n(r/min)	T_{av}(N·m)	TRR(%)	P_s(W)	P_d(W)	η(%)
Asymmetric Half Bridge	200	20	39.6	112.8	27.6	47.2
	800	15	38.8	78.2	20.7	78.5
	1500	10	58.9	25.6	9.1	83.7
Ring	200	20	37.5	90.9	25.2	52.9
	800	15	36.6	58.7	19.6	80.2
	1500	10	37.9	21.3	11.4	83.9
Ring with Extra Diodes	200	20	37.0	91.7	54.9	45.7
	800	15	36.2	55.2	44.6	78.4
	1500	10	37.7	22.3	31.9	82.5

The Torque Ripple Ratio (TRR) is defined:

$$TRR = \frac{T_{\max} - T_{\min}}{T_{av}} \times 100\% \tag{18}$$

The asymmetric half bridge converter exhibits reduced TRR at low and medium speed owing to the wider conduction width, whilst the ring converters exhibit reduced TRR at high speed as a result of the smoother current waveforms arising from the characteristic voltage angles.

V. EXPERIMENTAL VALIDATION

In order to test the proposed converters and compare them with a conventional asymmetric half bridge converter, a test rig is constructed with a six-phase SRM prototype, a load machine, power converters and a controller as shown in Fig. 17. Twelve fast switching IGBT modules are employed and mounted on the top of an air cooling heat sink as shown in Fig. 17(a). The components employed in the controller and drive are listed in Table V.

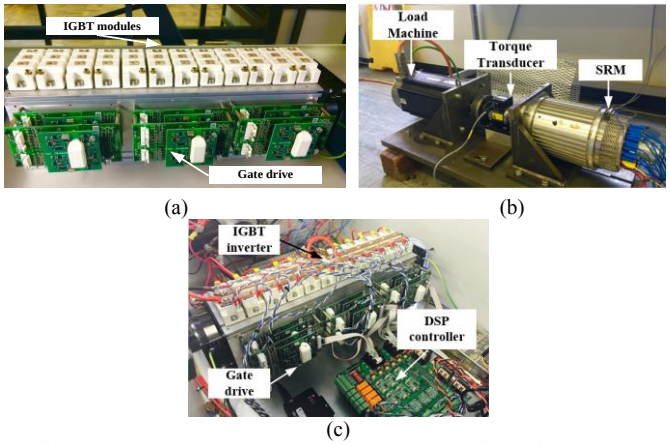

(a) (b) (c)

Fig. 17. Test rig construction. (a) Power converter. (b)Mechanical part. (c)Electrical part.

TABLE V.
EMPLOYED COMPONENTS IN THE CONTROLLER AND DRIVER

Component	Selected Model	Component	Selected Model
IGBT module 1	SKM150GAR12T4	DSP	TMS320F28335
IGBT module 2	SKM150GAL12T4	Gate driver	SKYPER 32 PRO R
Current transducer	LEM LA 55-P	Encoder	HENGSTLER AC58
Decoding chip	MAX1486EUB		

A. *Low speed test*

Fig. 18 shows experimental six phase current waveforms and torque waveform of the asymmetric half bridge converter. The presence (Fig. 19(a)) and absence (Fig. 19(b)) of any sharp distortions in the current waveforms at around 60° may be clearly observed in verification of the simulation and analysis work. Extended current tails are in evidence in both cases.

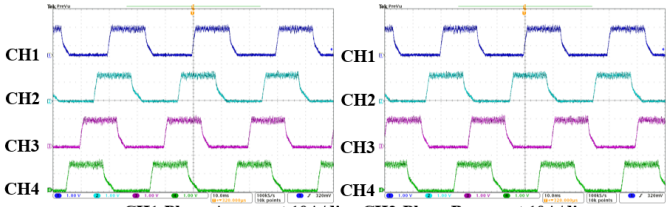

(a)

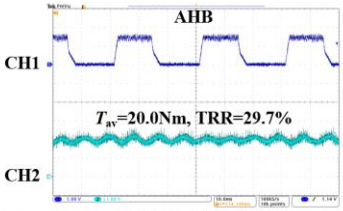

(b)

Fig. 18. Experimental waveforms of the asymmetric half bridge converter under current control.(a) Six phase current. (b) Torque.

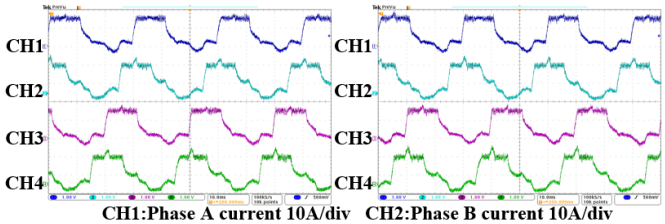

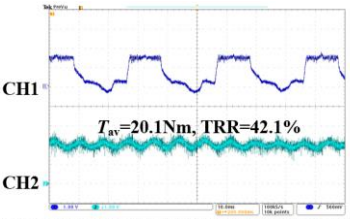

(a)

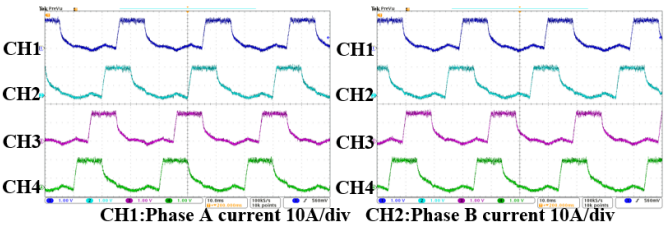

(b)

Fig. 19. Experimental waveforms of the ring converter under current control. (a)160° conduction width. (b)120° conduction width.

Fig. 20 shows the phase current waveforms measured with the ring converter with additional diodes with 120° conduction width. In this case, all the current distortions are avoided by comparison with Fig. 19(a). Owing to the conduction limitation, the TRR in Fig. 20(b) is 41.8%, greater than the asymmetric half bridge converter in Fig. 18(b).

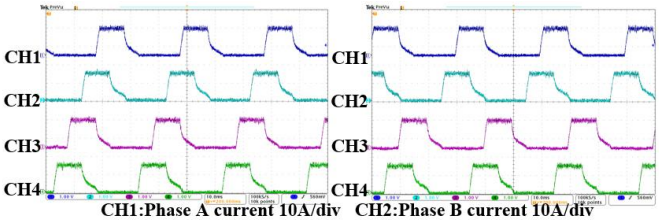

(a)

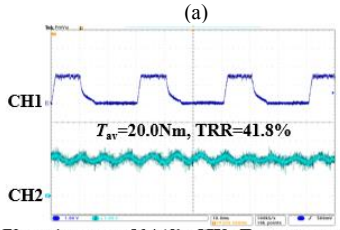

(b)

Fig. 20. Experimental waveforms of the ring converter with additional diodes under current control (200 r/min, 20 N·m). (a) Six phase current. (b) Torque.

B. *High speed test*

Fig. 21 shows the phase current and torque waveform, comparing the asymmetric half bridge converter with the proposed converters under voltage control at 1500 r/min, developing 10 N·m mean torque in all three cases. The TRR of the proposed converters is slightly lower, as predicted, owing to the characteristic voltage angles giving rise to a wider current waveform.

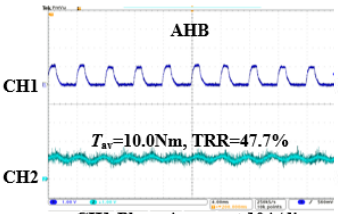

(a)

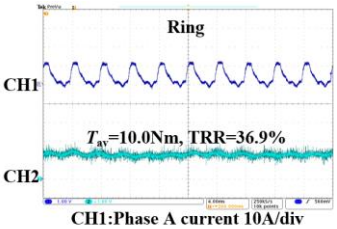

(b)

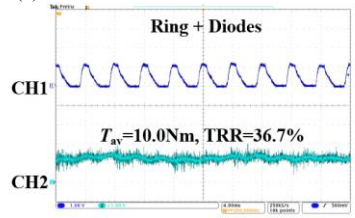

(c)

Fig. 21. Experimental phase current and torque waveforms under voltage control (1500r/min, 10Nm). (a) The asymmetric half bridge converter. (b)The ring converter. (c) The ring converter with additional diodes.

C. *Performance comparison*

The three different drives are compared on the bases of TRR and system efficiency at three different average torque settings,

T_{av}. System efficiency is calculated from the output mechanical energy P_m, and input energy P_e from the DC power supply. The parameters used and the results are summarized in Table VI. $\Delta\eta$ is the system efficiency error between simulation and experimental results.

TABLE VI.
EXPERIMENTAL PERFORMANCE COMPARISON

	n(r/min)	T_{av}(Nm)	TRR(%)	P_m(W)	P_e(W)	η(%)	$\Delta\eta$(%)
Asymmetric Half Bridge	200	20	29.7	194	418	46.3	0.9
	800	15	33.0	966	1256	76.9	1.6
	1500	10	47.7	1289	1570	82.1	1.6
Ring	200	20	42.1	211	418	50.4	2.5
	800	15	31.2	975	1256	77.6	2.6
	1500	10	36.9	1291	1570	82.2	1.7
Ring with Extra Diodes	200	20	27.5	180	418	43.1	2.6
	800	15	30.8	958	1256	76.3	1.9
	1500	10	36.7	1270	1570	80.9	1.6

The ring converter (without extra diodes) exhibits the highest efficiency throughout the speed range; this is most pronounced at low and medium speeds, where the fewer switches give reduced switching loss. The measurements verify the predictions of simulation and analysis. The asymmetric half bridge converter has lower TRR under current control owing to the increased conduction width allowed, whilst the ring converters have lower TRR at high speed owing to the smoother current waveforms shown in Fig. 21.

The ring converter with extra diodes suffers from the lowest efficiency. Although the extra diodes have been shown to successfully eliminate the current distortion after turn-off (Fig. 20(a)), the reduced efficiency and extra cost of this option confirm the ring converter without extra diodes as the preferred option in this case.

Experimental efficiency measurements are slightly lower than the simulation results predicted; the difference is ascribed to conduction losses in cables and auxiliary resistors, and other anomalous loss. Experimental TRR measurements are also slightly lower than the simulation results predicted; the difference is ascribed to the effects of mutual-inductance which are neglected in the simulation.

VI. CONCLUSION

This paper presents a ring converter topology for a six-phase SRM drive, without recourse to additional energy storage elements, requiring only six switches and six power connections, and facilitating a modified version of standard SRM control. Compared with the asymmetric half bridge converter, the number of switches and connections between the SRM and converter are reduced by half.

Conventional control methods are successfully modified and applied with the proposed ring converter throughout the whole speed range. However, owing to the phase interdependence arising from this configuration, the phase current exhibits two characteristic distortions, namely a sharp increase of current at around 60°, and an extended current tail after turn-off.

In order to avoid the former current distortion with the ring converter, a 120° conduction width limitation is imposed with good effect. In mitigation of the latter, the addition of a further six diodes is proposed for the ring converter, but this version is ultimately rejected due to increased continuous diode conduction loss.

By comparison with an asymmetric half bridge converter, the proposed ring converter evidences lower converter loss, fewer devices and higher system efficiency, and is therefore an attractive proposition for this application.

REFERENCES

[1] R. Madhavan and B. G. Fernandes, "Axial Flux Segmented SRM With a Higher Number of Rotor Segments for Electric Vehicles," *IEEE Transactions on Energy Conversion*, vol. 28, pp. 203-213, 2013.

[2] A. Chiba, K. Kiyota, N. Hoshi, M. Takemoto, and S. Ogasawara, "Development of a Rare-Earth-Free SR Motor With High Torque Density for Hybrid Vehicles," *IEEE Transactions on Energy Conversion*, vol. 30, pp. 175-182, 2015.

[3] Y. Sozer, I. Husain, and D. A. Torrey, "Guidance in Selecting Advanced Control Techniques for Switched Reluctance Machine Drives in Emerging Applications," *IEEE Transactions on Industry Applications*, vol. 51, pp. 4505-4514, 2015.

[4] M. Krishnamurthy, C. S. Edrington, A. Emadi, P. Asadi, M. Ehsani, and B. Fahimi, "Making the case for applications of switched reluctance motor technology in automotive products," *IEEE Transactions on Power Electronics*, vol. 21, pp. 659-675, 2006.

[5] I. Husain, "Minimization of torque ripple in SRM drives," *IEEE Transactions on Industrial Electronics*, vol. 49, pp. 28-39, 2002.

[6] S. Song, Z. Xia, Z. Zhang, and W. Liu, "Control Performance Analysis and Improvement of a Modular Power Converter for Three-Phase SRM With Y-Connected Windings and Neutral Line," *IEEE Transactions on Industrial Electronics*, vol. 63, pp. 6020-6030, 2016.

[7] A. Klein-Hessling, A. Hofmann, and R. W. D. Doncker, "Direct instantaneous torque and force control: a control approach for switched reluctance machines," *IET Electric Power Applications*, vol. 11, pp. 935-943, 2017.

[8] J. Lin, T. Lambert, Y. Yang, B. Bilgin, R. Lankin, and A. Emadi, "A novel axial flux switched reluctance motor with multi-level air gap geometry," in *2016 IEEE Electrical Power and Energy Conference (EPEC)*, 2016, pp. 1-8.

[9] Q. Sun, J. Wu, C. Gan, Y. Hu, N. Jin, and J. Guo, "A New Phase Current Reconstruction Scheme for Four-Phase SRM Drives Using Improved Converter Topology Without Voltage Penalty," *IEEE Transactions on Industrial Electronics*, vol. 45, pp. 1-10, 2017.

[10] C. Ma and L. Qu, "Multiobjective Optimization of Switched Reluctance Motors Based on Design of Experiments and Particle Swarm Optimization," *IEEE Transactions on Energy Conversion*, vol. 30, pp. 1144-1153, 2015.

[11] H. Eskandari and M. Mirsalim, "An Improved 9/12 Two-Phase E-Core Switched Reluctance Machine," *IEEE Transactions on Energy Conversion*, vol. 28, pp. 951-958, 2013.

[12] X. Deng, B. Mecrow, R. Martin, and S. Gadoue, "Effects of Winding Connection on Performance of a Six-Phase Switched Reluctance Machine," *IEEE Transactions on Energy Conversion*, vol. 33, pp. 166-178, 2018.

[13] Y. Jin, B. Bilgin, and A. Emadi, "An Offline Torque Sharing Function for Torque Ripple Reduction in Switched Reluctance Motor Drives," *IEEE Transactions on Energy Conversion*, vol. 30, pp. 726-735, 2015.

[14] R. B. Inderka and R. W. A. A. D. Doncker, "DITC-direct instantaneous torque control of switched reluctance drives," *IEEE Transactions on Industry Applications*, vol. 39, pp. 1046-1051, 2003.

[15] R. Mikail, I. Husain, M. S. Islam, Y. Sozer, and T. Sebastian, "Four-Quadrant Torque Ripple Minimization of Switched Reluctance Machine Through Current Profiling With Mitigation of Rotor Eccentricity Problem and Sensor Errors," *IEEE Transactions on Industry Applications*, vol. 51, pp. 2097-2104, 2015.

[16] D. H. Lee, Z. G. Lee, J. Liang, and J. W. Ahn, "Single-Phase SRM Drive With Torque Ripple Reduction and Power Factor Correction," *IEEE Transactions on Industry Applications*, vol. 43, pp. 1578-1587, 2007.

[17] X. Deng, B. Mecrow, H. Wu, and R. Martin, "Design and Development of Low Torque Ripple Variable-Speed Drive System With Six-Phase Switched Reluctance Motors," *IEEE Transactions on Energy Conversion*, vol. 33, pp. 420-429, 2018.

[18] J. A. Haylock, B. C. Mecrow, A. G. Jack, and D. J. Atkinson, "Operation of a fault tolerant PM drive for an aerospace fuel pump application," *IEE*

Proceedings on Electric Power Applications, vol. 145, pp. 441-448, 1998.
[19] X. Chen, J. Wang, V. I. Patel, and P. Lazari, "A Nine-Phase 18-Slot 14-Pole Interior Permanent Magnet Machine with Low Space Harmonics for Electric Vehicle Applications," *IEEE Transactions on Energy Conversion*, vol. 10, pp. 1-10, 2016.
[20] S. Vukosavic and V. R. Stefanovic, "SRM inverter topologies: a comparative evaluation," *IEEE Transactions on Industry Applications*, vol. 27, pp. 1034-1047, 1991.
[21] H. Lin, S. Hexu, G. Jie, and B. Jie, "Performance Research of Two Topologies of Power Converter for SRM," in *Power and Energy Engineering Conference*, 2012, pp. 1-4.
[22] E. Afjei, M. Asgar, and S. Ataei, "A New modified bifilar Drive Circuit for Switched Reluctance Motor," in *Joint International Conference on Power System Technology and IEEE Power India Conference*, 2008, pp. 1-4.
[23] R. Krishnan and P. N. Materu, "Design of a single-switch-per-phase converter for switched reluctance motor drives," *IEEE Transactions on Industrial Electronics*, vol. 37, pp. 469-476, 1990.
[24] Y. Hu, C. Gan, Q. Sun, P. Li, J. Wu, and H. Wen, "Modular Tri-Port High-Power Converter for SRM Based Plug-in Hybrid Electrical Trucks," *IEEE Transactions on Power Electronics*, vol. 33, pp. 3247-3257, 2018.
[25] Y. Hu, C. Gan, W. Cao, W. Li, and S. J. Finney, "Central-Tapped Node Linked Modular Fault-Tolerance Topology for SRM Applications," *IEEE Transactions on Power Electronics*, vol. 31, pp. 1541-1554, 2016.
[26] Y. Hu, C. Gan, W. Cao, J. Zhang, L. W, and S. J. Finney, "Flexible Fault-Tolerant Topology for Switched Reluctance Motor Drives," *IEEE Transactions on Power Electronics*, vol. 31, pp. 4654-4668, 2016.
[27] R. Martin, J. D. Widmer, B. C. Mecrow, M. Kimiabeigi, A. Mebarki, and N. L. Brown, "Electromagnetic Considerations for a Six-Phase Switched Reluctance Motor Driven by a Three-Phase Inverter," *IEEE Transactions on Industry Applications*, vol. 52, pp. 3783-3791, 2016.
[28] M. Barnes and C. Pollock, "Power electronic converters for switched reluctance drives," *IEEE Transactions on Power Electronics*, vol. 13, pp. 1100-1111, 1998.
[29] J. D. Widmer, B. C. Mecrow, C. M. Spargo, R. Martin, and T. Celik, "Use of a 3 phase full bridge converter to drive a 6 phase switched reluctance machine," in *6th IET International Conference on Power Electronics, Machines and Drives*, 2012, pp. 1-6.

Xu Deng received the B.Eng. and M.Eng. degrees in Electrical Engineering from Nanjing University of Aeronautics and Astronautics, Nanjing, China, in 2010 and 2013, respectively. She received the PhD degree in Electrical Engineering from Newcastle University, Newcastle upon Tyne, U.K, in 2017. She is currently a Research Associate of Electrical Power Research Group in the School of Engineering, Newcastle University, Newcastle upon Tyne, U.K. Her main researches are integrated drives and advanced control methods for power electronics and electric machines.

Barrie Mecrow received the Ph.D. degree in Electrical Engineering from Newcastle University, Newcastle, U.K., in 1986. He was a Turbo-generator Design Engineer at NEI Parsons, Newcastle upon Tyne, U.K. In 1987, he became a Lecturer and in 1998 a Professor at Newcastle University. His research interests include fault-tolerant drives, high-performance permanent magnet machines, and novel switched reluctance drives.

Haimeng Wu (M'10) was born in Zhejiang, China, in 1986. He received the B.Sc. degree in Electrical Engineering from Chongqing University, Chongqing, China, in 2008. He was nominated as the postgraduate exempted from the national postgraduate entrance examination to Zhejiang University and then he received the M.Sc. degree in Power Electronics from the College of Electrical Engineering, Zhejiang University, Hangzhou, China, in 2011. He received the grants from Engineering and Physical Science Council (EPSRC) for his further education in UK and he had his Ph.D. degree in Power Electronics at the School of Electrical and Electronic Engineering, Newcastle University, United Kingdom in 2016. He has been with the Electrical Power Research Group at Newcastle University as a Postdoctoral Researcher since 2015. His current research interests include power electronics for electric vehicles, design and advanced nonlinear control of power converters, health monitoring techniques.

Richard Martin received the M.Eng. degree in general engineering and the Ph.D. degree in Electrical Engineering from the University of Durham, Durham, U.K., in 2002 and 2007, respectively. He was a Research Associate with Newcastle University, Newcastle, U.K. from 2012 to 2016 and is now an Electromagnetic Design Engineer with Nidec SR Drives Ltd., Harrogate, U.K.

Yaohui Gai received the M.Sc. degree in electrical power engineering in 2015 from Newcastle University, Newcastle upon Tyne, U.K., where he is currently working toward the Ph.D. degree in electric power engineering. His research interests include thermal modeling, loss analysis, and cooling system design for the automotive traction electric motors.